CHAPTER «CHEMICAL SCIENCES»

NANOMATERIALS BASED ON CERIUM OXIDE AND DYSPROSIUM OXIDE DOPED WITH RARE-EARTH ELEMENT OXIDES (REVIEW)

НАНОМАТЕРІАЛИ НА ОСНОВІ ОКСИДУ ЦЕРІЮ ТА ДИСПРОЗІЮ ЛЕГОВАНОГО ОКСИДАМИ РІДКОЗЕМЕЛЬНИХ ЕЛЕМЕНТІВ (ОГЛЯД)

Olesia Pavlenko[1]

DOI: https://doi.org/10.30525/978-9934-26-631-7-9

Abstract. Cerium dioxide (CeO_2)–based nanomaterials are attracting increasing scientific interest due to their exceptional redox properties, oxygen storage capability, structural stability, and multifunctional catalytic behaviour. Doping CeO_2 with rare-earth oxides such as La_2O_3 and Dy_2O_3 enables targeted modification of its crystal structure, ionic conductivity, defect chemistry, and surface reactivity. *The purpose of the paper* is to summarize contemporary research on CeO_2–Dy_2O_3–La_2O_3 nanomaterials, focusing on their phase equilibria, defect formation, morphology-dependent catalytic activity, and photocatalytic performance. *Particular attention is given* to the fluorite-type lattice stability, dopant solubility limits (x_{max}), temperature-dependent phase relations, and the role of dysprosium in modulating oxygen-vacancy concentrations. Photocatalytic experiments on $Ce_{0.85}La_{0.10}Dy_{0.05}O_2$, synthesized at 800–1000 °C, demonstrate enhanced degradation efficiency of organic dyes under solar irradiation compared to undoped CeO_2. *The analysis highlights* the strong influence of dopant ionic radius, surface defect density, and nanostructure morphology on catalytic and photocatalytic performance. *The reviewed results* indicate that multicomponent CeO_2-based systems offer a promising platform for advanced catalysis, environmental remediation, energy-conversion devices, and functional ceramic materials.

[1] Ph.D in Chemistry, Senior Research Scientist,
Frantsevich Institute for Problems of Materials Science,
National Academy of Sciences of Ukraine, Ukraine

1. Introduction

The rapid development of contemporary materials science is driven by the demand for advanced materials whose properties surpass those of existing analogues. Cerium dioxide (CeO_2) has attracted exceptional attention due to its remarkable physical, chemical, and catalytic characteristics [1–14]. CeO_2 crystallizes in a cubic fluorite-type structure and functions as an n-type semiconductor with a band gap of approximately 3.02 eV, characterized by partially filled 4f orbitals.

The fluorite lattice enables efficient oxygen storage and release, which is fundamental to many technological applications [3].

Because of these features, CeO_2 is used in a wide range of fields, including hydrogenation processes [4], pharmaceutical technologies [5–6], removal of heavy metals [7], development of antimicrobial agents [9], electrolytes for solid-oxide fuel cells [6; 7], catalytic treatment of industrial gases [10–11], and solid-state lighting technologies [12].

A recent bibliometric evaluation [11] demonstrates a steady growth in global research interest in CeO_2-based materials (Fig. 1). In recent years, CeO_2 has emerged as a promising competitor to the widely used TiO_2 photocatalyst [11,13]. It is well established that catalytic activity depends not only on intrinsic physicochemical properties, but also on the exposure of specific crystallographic surfaces [11].

Compared with TiO_2, CeO_2 offers superior structural stability and unique redox behavior due to the 4f-electron configuration, which facilitates rapid oxygen exchange and the formation of abundant oxygen vacancies – key active sites for catalytic reactions [14].

2. Doping of Cerium Oxide with Rare-Earth elements

Enhancing the functional properties of cerium dioxide is commonly achieved through doping with rare-earth oxides. However, the dopant concentration must be carefully controlled to preserve the cubic fluorite structure. Phase-equilibrium studies in multicomponent systems based on CeO_2 provide accurate information on the concentration and temperature limits of the single-phase fluorite region [15–37].

For the binary systems CeO_2–La_2O_3 and CeO_2–Dy_2O_3, a broad and thermally stable homogeneous region exists between approximately 600 and 1500 °C (Fig. 2) [15; 34].

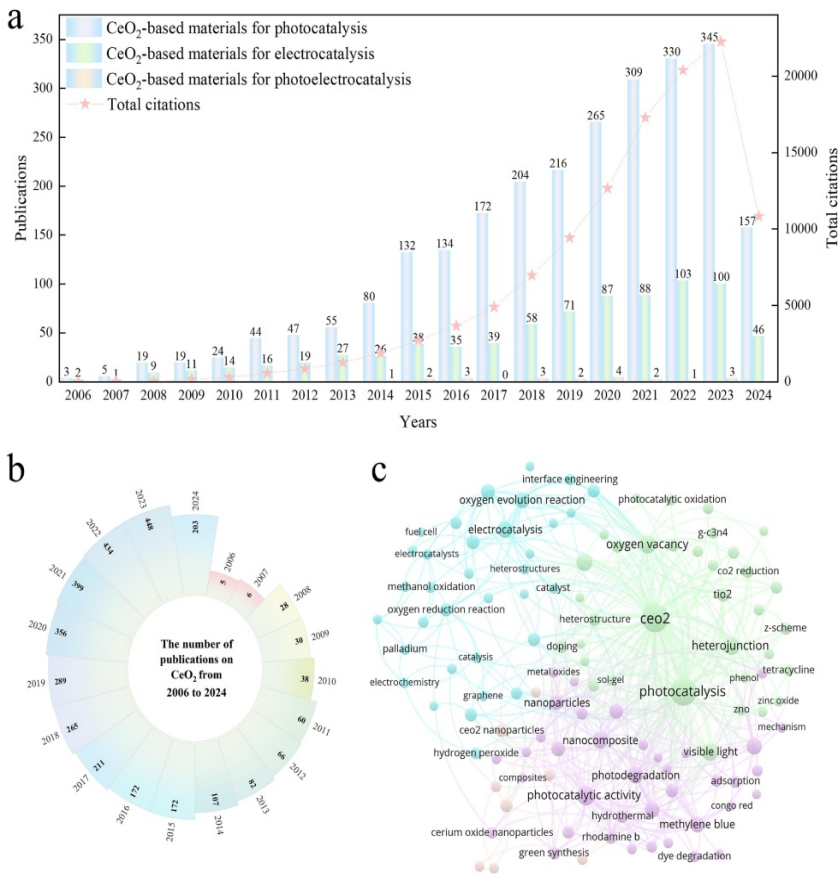

Figure 1 – a, b) number and citation trends of publications on CeO_2 photocatalysis, electrocatalysis, and photoelectrocatalysis from 2006 to 2024. c) bibliometric network visualization of CeO_2-related research topics

The functional behavior of nanomaterials based on CeO_2 doped with lanthanum or dysprosium is closely linked to the high oxygen diffusion coefficient and the ability of cerium – both pure and doped – to undergo reversible oxygen exchange with the surrounding atmosphere. Dysprosium

oxide is widely used in high-performance Nd–Fe–B permanent magnets to improve their thermal stability.

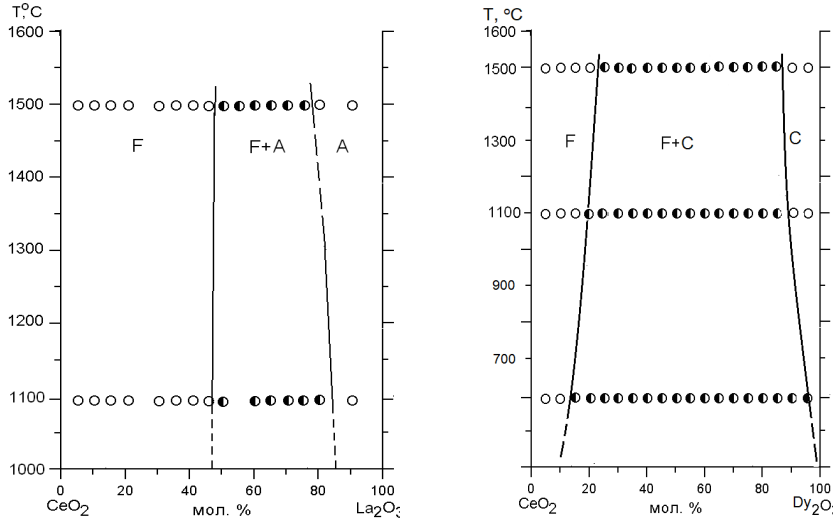

a b

Figure 2. Phase equilibria:(a) the CeO_2–La_2O_3 system [15], (b) the CeO_2–Dy_2O_3 system [34]

Several comprehensive reviews on doped ceria [38–44] highlight the exceptional versatility of CeO_2-based materials and their potential impact across catalysis, optics, energy conversion, and environmental remediation. These works span fundamental structure–property relationships, synthesis and characterization techniques, theoretical modeling, and emerging catalytic mechanisms.

3. Morphology-dependent catalytic behavior of doped Cerium oxide

The catalytic applications of nanomaterials based on cerium oxide doped with lanthanum and dysprosium have been examined in detail in [40]. Nanoparticles of these materials are frequently employed either as active catalytic components or as supports across a variety of reactions. Their catalytic performance is strongly morphology-dependent: particle

shape, exposed facets, and defect structures influence reaction pathways and activity.

The study discusses how the morphology of doped CeO_2 affects catalytic oxidation of carbon monoxide, reduction of nitrogen oxides, and various reforming reactions. The surface structure of dysprosium oxide – when incorporated as a dopant – plays an important role in determining catalytic activity and selectivity due to its influence on surface geometry, defect density, and the energy required to form oxygen vacancies.

The authors propose a strategy for fine-tuning catalytic performance by controlling nanoparticle shape without altering the chemical composition. Doped CeO_2 also functions effectively as an electrolyte because the fluorite-type lattice can sustain a high concentration of mobile oxygen vacancies. For this reason, determining the maximum dopant concentration (x_{max}) that can be incorporated into the fluorite lattice while maintaining single-phase homogeneity is essential.

Maximum solubility limits of Rare-Earth dopants in CeO_2. Figure 3 illustrates the relationship between ionic radius and dopant coordination for various rare-earth elements. The red guidelines indicate the approximate upper and lower boundaries of x_{max} reported for each dopant. The x_{max} value is defined as the composition midpoint between the highest dopant concentration still forming a single-phase fluorite structure and the composition at which a secondary phase first appears [45].

The data show substantial variation in x_{max}, particularly for dopants of intermediate ionic radius. Elevated x_{max} values reported in some studies are attributed to high-temperature synthesis ($T \geq 1600$ °C), which may not reflect equilibrium solubility at lower temperatures. Above ~1500 °C, phase separation can occur, leading to partial decomposition of the solid solution into individual oxides

4. Influence of Dy on ionic conductivity in Ce-based electrolytes

The effect of dysprosium incorporation into CeO_2-based electrolytes was investigated in [46]. The results show that Dy^{3+} increases ionic conductivity and decreases activation energy compared to the widely used samarium-doped ceria composition $Ce_{0.8}Sm_{0.2}O_{2-\delta}$ (SDC) over the temperature range 300–800 °C.

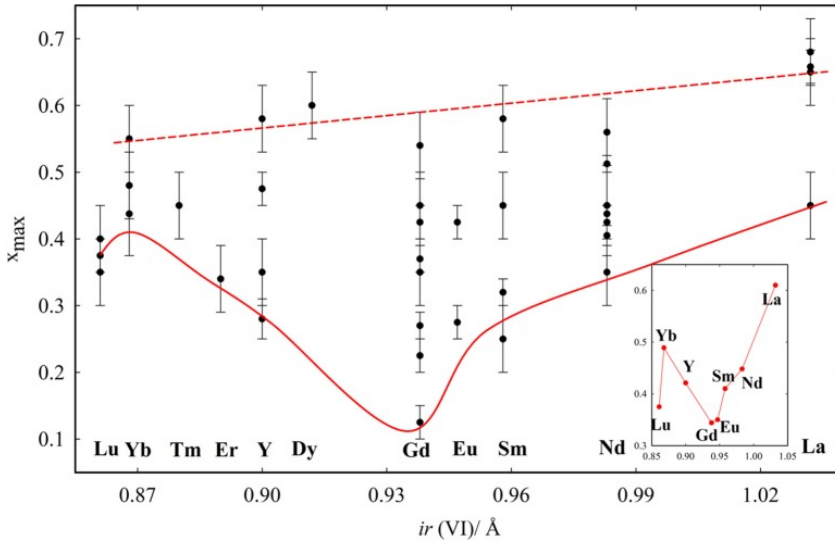

Figure 3. Graphical representation of x_{max} values for various rare-earth dopants [45]

At 2 mol% Dy_2O_3 (composition $Ce_{0.8}Sm_{0.18}Dy_{0.02}O_2$-δ), the highest ionic conductivity was obtained. Dysprosium strongly affects grain-boundary conductivity, while its influence on bulk conductivity is less pronounced. X-ray diffraction confirms that all samples remain single-phase fluorite structures. Thermal expansion behavior is linear, and Dy^{3+} addition does not significantly modify the thermal expansion coefficient, which remains in the range (12.62–13.05) × 10^{-6} K^{-1}.

Optical and Luminescent Properties of Dy-Doped CeO_2. Photoluminescence properties of CeO_2 doped with Dy^{3+} ions were examined in [47], demonstrating that Dy-doped CeO_2 is a promising candidate for display technologies and optical devices. In [48], pure and Dy_2O_3-doped CeO_2 nanoparticles were synthesized using a microwave-assisted method. The purpose of doping was to enhance chemical stability, optical absorption, and fluorescence intensity.

X-ray diffraction confirmed the formation of composite structures containing Dy^{3+}/Ce^{3+} in a cubic lattice with average crystallite sizes of 16–22 nm. The results show a significant enhancement of fluorescence emission in Dy-doped samples compared with undoped CeO_2.

Magnetic properties of rare-earth-doped Ceria. The magnetic properties of CeO_2 doped with various rare-earth ions (Nd, Sm, Gd, Tb, Er, Dy) were investigated in [49]. Room-temperature ferromagnetism was observed in heat-treated CeO_2 samples doped with Nd and Sm, whereas samples doped with Gd, Tb, Er, or Dy exhibited paramagnetic behavior.

The origin of magnetism is attributed to oxygen vacancies and the fluorite-type crystal structure. The study also evaluates the impact of dopant concentration (1, 5, and 15%) on magnetic response for Gd, Tb, Er, and Dy additives.

5. Photocatalytic oxidation of organic pollutants using CeO_2- and Dy_2O_3-based materials

The rapid expansion of industrial activity has resulted in the increased release of toxic organic contaminants – including synthetic dyes – into natural water systems. Wastewater containing pollutants such as erythrosine, thymol blue, methyl orange, malachite green, and rhodamine B is of particular concern because these compounds exhibit low biodegradability and pose environmental and health risks [50].

Photocatalysis offers an effective route for degrading such pollutants by harnessing solar energy to drive oxidative decomposition reactions [51]. Solar-driven photocatalysis requires no additional chemicals or external energy inputs, making it a sustainable method for wastewater treatment. With growing demand for efficient removal of hazardous organic pollutants, the design of high-performance nanostructured photocatalysts has become a major focus in environmental materials research [52].

A wide range of nanostructures and nanocomposites has been explored for photocatalytic purification of dye-contaminated water [53]. However, there remains a strong need for new materials with higher efficiency and stability. Dysprosium oxide (Dy_2O_3) is of particular interest due to its exceptional thermal stability and low solubility [54; 55], as well as its promising optical and catalytic characteristics [56–60]. Dy_2O_3 possesses a wide band gap of approximately 4.8 eV [61], but its photocatalytic

properties can be improved by forming composites – for example with ZnO – to enhance light absorption and modify electronic structure [61].

Multiple synthetic methods have been reported for Dy_2O_3 nanostructures, including precipitation [55], thermal decomposition [63], combustion synthesis [56], and sol–gel processing [54], among others.

6. Photocatalytic performance of Dy_2O_3–SiO_2 and La_2O_3-Ag_3VO_4 nanocomposites

Table 1 summarizes the photocatalytic efficiency of different nanostructured systems for the degradation of several organic dyes under UV irradiation [52]. As shown, Dy_2O_3–SiO_2 nanocomposites fabricated via a sonochemical route exhibit competitive photocatalytic activity compared with widely studied oxide photocatalysts.

The photocatalytic activity of Dy_2O_3 nanoparticles was further evaluated for malachite green degradation under UV illumination [67]. The catalyst achieved 92.76% degradation within 120 minutes at an optimal mass loading of 5 mg, exhibiting excellent stability with only minimal loss of activity after four cycles. The degradation followed first-order kinetics with a rate constant $k_{app} = 2.04 \times 10^{-2}$ min^{-1}. Trapping experiments revealed that photogenerated holes (h^+) play the dominant role in the degradation mechanism.

Photocatalytic Enhancement in La_2O_3/Ag_3VO_4 composites. The influence of lanthanum content on the photocatalytic activity of La_2O_3/Ag_3VO_4 composites is shown in Fig. 4 [68]. Under visible light irradiation (553 nm), the pure Ag_3VO_4 and P25 TiO_2 catalysts exhibit RhB degradation efficiencies of 51% and 23%, respectively, after 60 minutes. Upon the introduction of La^{3+}, the photocatalytic activity is significantly enhanced across all compositions.

This improvement is attributed to the red-shift in light absorption: the absorption edge of the La_2O_3/Ag_3VO_4 composite shifts toward longer wavelengths, enabling more efficient utilization of visible light. Enhanced photon absorption correlates directly with increased photocatalytic degradation efficiency. As noted in [69], a substantial red-shift is indicative of improved light-harvesting capacity, which boosts photocatalytic activity.

Table 1

Comparison of photocatalytic efficiency for the degradation of various pollutants between the Dy_2O_3–SiO_2 nanocomposite and other compounds under ultraviolet irradiation [52]

Material	Pollutant	Efficiency (%) & Time (min)
$La_2Sn_2O_7$	Erythrosine	84% in 120 min
TiO_2-P25	Methyl orange	90.5% in 180 min
TiO_2	Acid Red 14	88% in 150 min
CdS	Eriochrome	42% in 60 min
ZnO–CdO	Thymol blue	46% in 120 min
Dy_2O_3–SiO_2	Malachite green	71.08% in 120 min
Dy_2O_3–SiO_2	Methyl orange	71.43% in 120 min
Dy_2O_3–SiO_2	Erythrosine	92.99% in 120 min

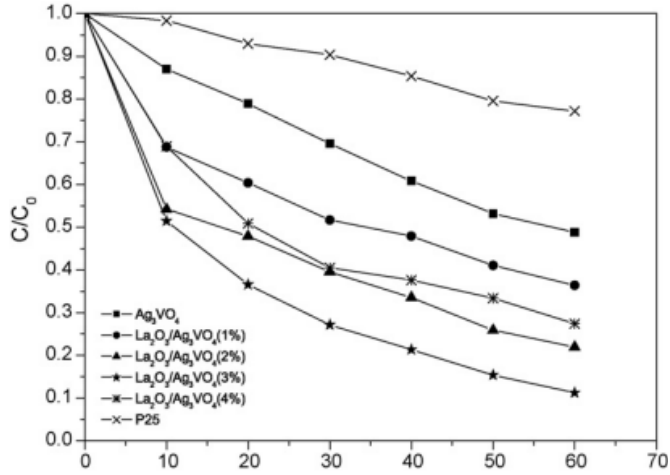

Figure 4. Photocatalytic activity of La_2O_3/Ag_3VO_4 (0.5 g/L) at different La^{3+} contents [68]

7. Adsorption and photocatalytic behavior of CeO_2 nanoparticles and La–Dy–CeO_2 ternary oxides

Adsorption and photocatalytic behavior of CeO_2 nanoparticles. In [70], CeO_2 nanoparticles synthesized via a sol–gel method was evaluated for the removal of indigo carmine and methylene blue under visible light

irradiation. The highest color removal efficiency was observed for indigo carmine (≈ 90% at pH 2.5 after 180 minutes), demonstrating that CeO_2 nanoparticles are effective for degrading anionic dyes at room temperature.

Color removal efficiency was calculated using equation (1.1), adapted from [71]:

$$color\ removal\ (\%) = \left(\frac{(C_0 - C)}{C_0}\right) x\ 100 = \left(\frac{(A_0 - A)}{A_0}\right) x\ 100 \qquad (1.1)$$

where C_0 and C refer to the initial and changing concentrations of the dye solution, respectively. A_0 represents the initial absorbance, and A – at a predetermined time.

Heterogeneous photocatalytic degradation of organic dyes typically proceeds through five key steps [72–74]:

1) Mass transfer of dye molecules from solution to the catalyst surface.

2) Adsorption of dye molecules onto CeO_2.

3) Photoexcitation followed by oxidation–reduction reactions involving adsorbed species.

4) Desorption of degradation products from the catalyst surface.

5) Diffusion of products into the bulk solution.

Adsorption capacity plays a decisive role in determining the degradation rate [75]. For this reason, the authors of [70] investigated dye adsorption onto CeO_2 nanoparticles at varying pH levels to better understand the relationship between surface chemistry and photocatalytic performance.

Photocatalytic behavior of La–Dy–CeO_2 ternary oxides. A detailed study of photocatalytic performance in La–Dy–CeO_2 ternary oxides is presented in [1]. The authors synthesized $Ce_{0.85}La_{0.10}Dy_{0.05}O_2$ using a sol–gel method followed by heat treatment at 800 °C and 1000 °C to investigate the impact of dopants and calcination temperature on photocatalytic activity.

The incorporation of lanthanum and dysprosium into the CeO_2 lattice significantly alters the structural and optical properties of the material. Doping introduces lattice distortions and enhances the concentration of oxygen vacancies – defects that are essential active sites for photocatalytic reactions. Increasing the calcination temperature results in improved crystallinity but also affects surface area, defect density, and, consequently, photocatalytic performance.

The degradation activity of the photocatalysts under sunlight is shown in Fig. 5. Undoped CeO_2 exhibits moderate photocatalytic efficiency. However,

the ternary oxide $Ce_{0.85}La_{0.10}Dy_{0.05}O_2$ demonstrates substantially higher photocatalytic degradation rates for the model dye pollutant, especially after calcination at 800 °C.

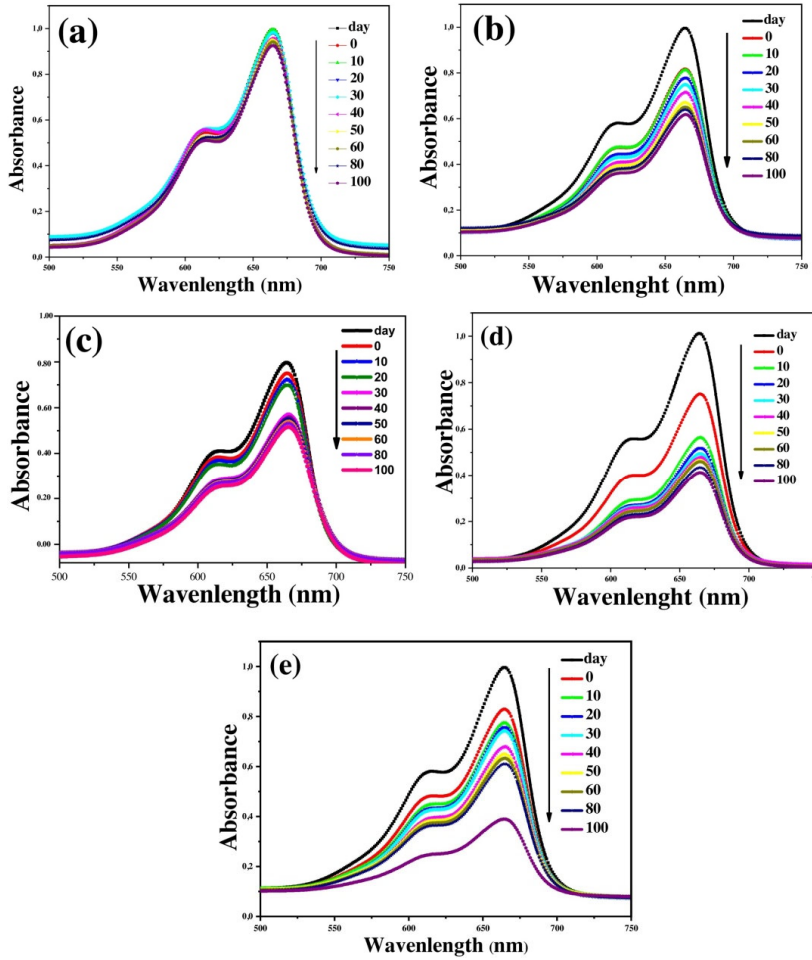

Figure 5. Degradation activity of photocatalysts (60 mg): (a) sun; (b) undoped CeO_2, 800 °C; (c) undoped CeO_2, 1000 °C; (d) $Ce_{0.85}La_{0.10}Dy_{0.05}O_2$, 800 °C; (e) $Ce_{0.85}La_{0.10}Dy_{0.05}O_2$,1000 °C

Two main factors contribute to this enhancement:

1. Increased oxygen vacancy concentration. Dopant ions La^{3+} and Dy^{3+} have larger ionic radii compared with Ce^{4+}, leading to lattice expansion and the formation of additional oxygen vacancies for charge compensation. These vacancies act as electron traps that prevent rapid electron–hole recombination, thereby increasing photocatalytic efficiency.

2. Improved absorption of visible light. Doping causes slight band-gap modification and introduces localized defect states that enhance visible-light absorption. This makes the material more responsive to solar irradiation compared with undoped CeO_2, which primarily absorbs UV light.

The photocatalytic performance hierarchy reported in [1] corresponds to sunlight irradiation: $Ce_{0.85}La_{0.10}Dy_{0.05}O_2$ (800 °C) > $Ce_{0.85}La_{0.10}Dy_{0.05}O_2$ (1000 °C) > undoped CeO_2. This demonstrates that the ternary doped system offers synergistic advantages beyond what La-doped or Dy-doped CeO_2 can achieve individually. The combination of optimized dopant concentrations and moderate calcination temperature yields a material with high photocatalytic performance and stable structural properties.

Conclusions

The conducted analysis demonstrates that cerium dioxide is a highly functional material whose properties can be substantially modified through doping with rare-earth oxides. The incorporation of dysprosium and lanthanum oxides stabilizes the fluorite-type lattice, promotes the formation of additional oxygen vacancies, and enhances the overall functional performance of the material. It has been established that the solubility limits of rare-earth dopants in the CeO_2 lattice depend on their ionic radii and the thermal conditions of synthesis, which makes it possible to predict the structural behavior, stability of the solid solutions, and their high-temperature performance. This provides a foundation for the targeted design of materials with controllable physicochemical properties.

Particular attention has been given to the influence of nanoparticle morphology on their catalytic and photocatalytic activity. The results indicate that variations in surface structure, grain size, aggregation degree, and defect density lead to significant changes in functional behavior. Notably, the $Ce_{0.85}La_{0.10}Dy_{0.05}O_2$ composition exhibits markedly improved photocatalytic efficiency in the degradation of organic dyes compared

with undoped CeO_2. This enhancement arises not only from the increased concentration of oxygen vacancies but also from improved adsorption of dye molecules, more efficient charge transport, and the enhanced formation of reactive radicals under irradiation.

Overall, the findings confirm that multicomponent CeO_2-based nanomaterials doped with Dy_2O_3 and La_2O_3 hold significant promise for use in modern catalytic systems, environmental remediation technologies, sensor devices, and energy-conversion applications. Their structural stability, tunable defect chemistry, and capacity to activate surface processes make them strong candidates for the development of advanced functional nanomaterials with a broad range of technological and ecological uses.

References:

1. Handan Özlü Torun, Rabia Kırkgeçit, Fatma Kılıç Dokan, & Esra Öztürk. (2021). Preparation of La-Dy-CeO_2 ternary compound: Examination of photocatalytic and photoluminescence properties. *Journal of Photochemistry and Photobiology A: Chemistry, 418*, 113338. https://doi.org/10.1016/j.jphotochem.2021.113338

2. Balakrishnan, G., Raghavan, C. M., Ghosh, C., Divakar, R., Mohandas, E., Song, J. I., & Kim, G. (2013). X-ray diffraction, Raman and photoluminescence studies of nanocrystalline cerium oxide thin films. *Ceramics International, 39*(7), 8327–8333.

3. Horovistiz, A. L., Rocha, R. A., & Muccillo, E. N. S. (2013). Electrical conductivity and microstructure relationship in ternary systems based on cerium oxide. *Ceramics International, 39*, 5887–5892. https://doi.org/10.1016/j.ceramint.2013.01.008

4. Shi, Z., Tan, Q., & Wu, D. (2018). Ternary copper-cerium-zirconium mixed metal oxide catalyst for direct CO_2 hydrogenation to methanol. *Materials Chemistry and Physics, 219*, 263–272. https://doi.org/10.1016/j.matchemphys.2018.08.038

5. Calvache-Muñoz, J., Prado, F. A., & Rodríguez-Páez, J. E. (2017). Cerium oxide nanoparticles: Synthesis, characterization and tentative mechanism of particle formation. *Colloids and Surfaces A: Physicochemical and Engineering Aspects, 529*, 146–159.

6. Xu, C., Lin, Y., Wang, J., Wu, L., Wei, W., Ren, J., & Qu, X. (2013). Nanoceria-triggered synergetic drug release based on CeO_2-capped mesoporous silica host-guest interactions and switchable enzymatic activity and cellular effects of CeO_2. *Advanced Healthcare Materials, 2*, 1591–1599.

7. Priyadharsan, A., Vasanthakumar, V., Karthikeyan, S., Raj, V., Shanavas, S., & Anbarasan, P. M. (2017). Multi-functional properties of ternary CeO_2/SnO_2/rGO nanocomposites: Visible light driven photocatalyst and heavy metal removal. *Journal of Photochemistry and Photobiology A: Chemistry, 346*, 32–45. https://doi.org/10.1016/j.jphotochem.2017.05.030

8. Li, X., Qi, M., Sun, X., Weir, M. D., Tay, F. R., Oates, T. W., Dong, B., Zhou, Y., Wang, L., & Xu, H. H. K. (2019). Surface treatments on titanium implants via nanostructured ceria for antibacterial and anti-inflammatory capabilities. *Acta Biomaterialia, 94*, 627–643. https://doi.org/10.1016/j.actbio.2019.06.023

9. Özlü Torun, H., & Çakar, S. (2018). Thermal characterization of Er-doped and Er–Gd co-doped ceria-based electrolyte materials for SOFC. *Journal of Thermal Analysis and Calorimetry, 133*, 1233–1239. https://doi.org/10.1007/s10973-018-7189-8

10. Govinda Rao, B., Jampaiah, D., Venkataswamy, P., & Reddy, B. M. (2016). Enhanced catalytic performance of manganese and cobalt Co-doped CeO_2 catalysts for diesel soot oxidation. *ChemistrySelect, 1*, 6681–6691. https://doi.org/10.1002/slct.201601297

11. Zhang, Y., Zhou, Y., Sun, D., Nie, Y., Wu, D., Ban, L., Tang, B., Yang, S., Li, H., Ma, T., & Zhang, H. (2025). CeO_2-based functional materials: Advancing photo- and electro-driven catalysis for environmental remediation and energy conversion. *Coordination Chemistry Reviews, 527*, 216395. https://doi.org/10.1016/j.ccr.2024.216395

12. Basavaraj, R. B., Navami, D., Deepthi, N. H., Venkataravanappa, M., Lokesh, R., Sudheer Kumar, K. H., & Sreelakshmi, T. K. (2020). Novel orange-red emitting Pr^{3+} doped CeO_2 nanopowders for white light emitting diode applications. *Inorganic Chemistry Communications, 120*, 108164. https://doi.org/10.1016/j.inoche.2020.108164

13. Xue, L., Zhang, C., Wu, J., Fan, Q.-Y., Liu, Y., Wu, Y., Li, J., Zhang, H., Liu, F., & Zeng, S. (2022). Unveiling the reaction pathway on Cu/CeO_2 catalyst for electrocatalytic CO_2 reduction to CH_4. *Applied Catalysis B: Environmental, 304*, 120951. https://doi.org/10.1016/j.apcatb.2021.120951

14. Yan, Y.-Q., Wu, Y.-Z., Wu, Y.-H., Weng, Z.-L., Liu, S.-J., Liu, Z.-G., Lu, K.-Q., & Han, B. (2024). Recent advances of CeO_2-based composite materials for photocatalytic applications. *ChemSusChem, 17*(14). https://doi.org/10.1002/cssc.202301778

15. Andrievskaya, E. R., Kornienko, O. A., Sameljuk, A. V., & Sayir, A. (2011). Phase relation studies in the CeO_2–La_2O_3 system at 1100–1500 °C. *Journal of the European Ceramic Society, 31*, 1277–1283. http://dx.doi.org/10.1016/j.jeurceramsoc.2010.05.024

16. Andrievskaya, E. R., Kornienko, O. A., & Gorodov, V. S. (2008). Phase relations in the CeO_2–Sm_2O_3 system at 1500 °C. *Current Problems of Physical Material Science, 17*, 25–29.

17. Andrievskaya, E. R., Gusarov, V. V., Kornienko, O. A., & Sameljuk, A. V. (2012). Interaction of ceria and erbia at 1500 °C. *Proceedings of Berezhnyi Institute for Refractories, 112*, 133–140.

18. Andrievskaya, E. R., Kornienko, O. A., Bykov, O. I., Sameliuk, A. V., & Bohatyriova, Z. D. (2019). Interaction of ceria and ytterbia in air within temperature range 600–1500 °C. *Journal of the European Ceramic Society, 39*, 2930–2935.

19. Andrievskaya, E. R., Kornienko, O. A., Sameljuk, A. V., & Sayir, A. (2020). Phase relation studies in the CeO_2–Eu_2O_3 system at 600–1500 °C. *Journal of the European Ceramic Society, 40*(3), 751–758.

20. Kornienko, O. A., Yushkevych, S. V., Bykov, O. I., Samelyuk, A. V., Bataiev, Y. M., & Zamula, M. V. (2023). Phase relation studies in the CeO_2–La_2O_3–Ho_2O_3 system at temperature of 1500 °C. *Materials Today Communications, 35*, 105789. https://doi.org/10.1016/j.mtcomm.2023.105789

21. Andrievska, O. R., Kornienko, O. A., & Yurchenko, Yu. V. (2020). Phase relation studies in the CeO_2–Sm_2O_3 system at 1500 to 600 °C in air. *Research & Development in Material Science, 12*(4), 1308–1314. https://doi.org/10.31031/RDMS.2020.12.000795

22. Kornienko, O. A., Bykov, O. I., Sameljuk, A. V., Bataiev, Yu. M., & Yushkevych, S. V. (2021). Phase equilibria in the CeO_2–La_2O_3–Gd_2O_3 system at 1250 and 1500 °C. *International Research Journal of Multidisciplinary Technovation, 3*(4), 17–31. https://doi.org/10.34256/irjmt2143

23. Kornienko, O. A., Bykov, O. I., Samelyuk, A. V., & Barshchevska, H. K. (2021). Isothermal section of the phase diagram of the CeO_2–La_2O_3–Sm_2O_3 system at 1500 °C. *Journal of Chemistry and Technologies, 29*(2), 200–210. https://doi.org/10.15421/jchemtech.v29i2.230369

24. Kornienko, O., Yushkevych, S., Bykov, O., Samelyuk, A., & Bataiev, Y. (2022). Phase equilibrium in the ternary CeO_2–La_2O_3–Yb_2O_3 system at 1500 °C. *Solid State Phenomena, 331*, 159–172. https://doi.org/10.4028/p-4000g3

25. Kornienko, O. A., Yushkevych, S. V., Bykov, O. I., Samelyuk, A. V., Bataiev, Yu. M., & Zamula, M. V. (2022). Phase equilibrium in binary La_2O_3–Dy_2O_3 and ternary CeO_2–La_2O_3–Dy_2O_3 systems. *Journal of the European Ceramic Society, 42*, 5820–5830. https://doi.org/10.1016/j.jeurceramsoc.2022.06.045

26. Andrievskaya, O. R., Kornienko, O. A., Bykov, O. I., Chudinovic, O. V., & Spasonova, L. N. (2021). The interaction between cerium dioxide, lanthanum, and europium oxides at 1500 °C. *Processing and Application of Ceramics, 15*(1), 32–39. https://doi.org/10.2298/PAC2101032A

27. Kornienko, O. A., Sameljuk, A. V., Bykov, O. I., Yurchenko, Yu. V., & Barshchevskaya, A. K. (2020). Phase relation studies in the CeO_2–La_2O_3–Er_2O_3 system at 1500 °C. *Journal of the European Ceramic Society, 40*(12), 4184–4190. https://doi.org/10.1016/j.jeurceramsoc.2020.04.042

28. Kornienko, O. A., Bykov, O. I., Samelyuk, A. V., & Yurchenko, Yu. V. (2020). Isothermal section of the phase diagram of the CeO_2–La_2O_3–Eu_2O_3 system at 1250 °C. *Ukrainian Chemical Journal, 86*(3), 35–47. https://doi.org/10.33609/0041-6045.86.3.2020.35-47

29. Hrovat, M., Holc, J., Bernik, S., & Makovec, D. (1998). Subsolidus phase equilibria in the NiO–CeO_2 and La_2O_3–CeO_2–Fe_2O_3 systems. *Materials Research Bulletin, 33*(8), 1175–1183. https://doi.org/10.1016/S0025-5408(98)00103-2

30. Ivas, T., Povoden-Karadeniz, E., Grundy, N. S., Jud-Sierra, E., Grässlin, J., & Gauckler, L. J. (2013). Experimental phase diagram determination and thermodynamic assessment of the CeO_2–Gd_2O_3–CoO system. *Journal of the American Ceramic Society, 96*, 613–626. https://doi.org/10.1111/jace.12004

31. Kornienko, O. A., Andrievskaya, O. R., & Barshchevskaya, H. K. (2020). Phase relations in the ternary system based on ceria, zirconia, and ytterbia at 1500 °C. *Journal of Chemistry and Technologies*, № 2, 142–152. https://doi.org/10.15421/082015

32. Andrievskaya, E. R., Kornienko, O. A., Sayir, A., Vasylkiv, O. O., & Sakka, Yoshio. (2011). Phase relation studies in the ZrO_2–CeO_2–La_2O_3 system at 1500 °C. *Journal of the American Ceramic Society, 94*(6), 1911–1919. https://doi.org/10.1111/j.1551-2916.2010.04316.x

33. Kornienko, O. A., Bykov, A. I., Andrievskaya, E. R., et al. (2020). Phase equilibria in the ZrO_2–CeO_2–Yb_2O_3 system at 1100 °C. *Powder Metallurgy and Metal Ceramics, 59*, 342–349. https://doi.org/10.1007/s11106-020-00167-0

34. Kornienko, O. A., & Andrievskaya, O. R. (2020). Phase equilibria in the systems with ZrO_2, CeO_2, and Dy_2O_3. In *Innovative Scientific Researches: European Development Trends and Regional Aspect* (4th ed., pp. 260). Riga, Latvia: Baltija Publishing. https://doi.org/10.30525/978-9934-588-38-9-58

35. Yushkevych, S., & Korichev, S. (2024). Phase equilibria in the CeO_2–Nd_2O_3 system at 1500 °C. Riga: Baltija Publishing.

36. Yushkevych, S. V., Kornienko, O. A., Bykov, O. I., & Subota, I. S. (2023). Isothermal section of the phase diagram of the ternary CeO_2–La_2O_3–Dy_2O_3 system at 1100 °C. *Journal of Chemistry and Technologies, 31*(2). https://doi.org/10.15421/jchemtech.v31i2.275434

37. Andrievskaya, E. R., Gerasimyuk, G. I., Kornienko, O. A., et al. (2006). Phase equilibria in the system HfO_2–ZrO_2–CeO_2 at 1500 °C. *Powder Metallurgy and Metal Ceramics, 45*, 448–456. https://doi.org/10.1007/s11106-006-0105-y

38. Montini, T., Melchionna, M., Monai, M., & Fornasiero, P. (2016). Fundamentals and catalytic applications of CeO_2-based materials. *Chemical Reviews, 116*, 5987–6041.

39. Trovarelli, A., & Llorca, J. (2017). Ceria catalyst at the nanoscale: How do crystal shapes shape catalysis? *ACS Catalysis, 7*, 4716–4735.

40. Qiao, Z. A., Wu, Z., & Dai, S. (2013). Shape-controlled ceria-based nanostructures for catalysis applications. *ChemSusChem, 6*(10), 1821–1833.

41. Ainscough, J. B., Moore, D. A., & Osborn, S. C. (1975). The kinetics of the C → B transformation in europium sesquioxide. *Journal of Nuclear Materials, 55*, 229–232.

42. Grover, V., & Tyagi, A. K. (2004). Phase relations, lattice thermal expansion in CeO_2–Gd_2O_3 system, and stabilization of cubic gadolinia. *Materials Research Bulletin, 39*, 859–866.

43. Mandal, B. P., Grover, V., & Tyagi, A. K. (2006). Phase relations, lattice thermal expansion in $Ce_{1-x}Eu_xO_{2-x/2}$ and $Ce_{1-x}Sm_xO_{2-x/2}$ systems and stabilization of cubic RE_2O_3 (RE: Eu, Sm). *Materials Science and Engineering A, 430*, 120–124.

44. Guo, B., Harvey, A., Risbud, S. H., & Kennedy, I. M. (2006). The formation of cubic and monoclinic Y_2O_3 nanoparticles in a gas-phase flame process. *Philosophical Magazine Letters, 86*, 457–467.

45. Coduri, M., Checchia, S., Longhi, M., Ceresoli, D., & Scavini, M. (2018). Rare earth doped ceria: The complex connection between structure and properties. *Frontiers in Chemistry, 6*, 526.

46. Yifeng, Z., Ming, Z., et al. (2010). Effect of Dy on the properties of Sm-doped ceria electrolyte for IT-SOFCs. *Journal of Alloys and Compounds, 509*(4).

47. Jagjeet, K., Deepika, C., Vikas, D., Ravi, S., Yogita, P., & Suryanarayana, N. S. (2016). Photoluminescence characteristics of dysprosium doped CeO_2 phosphor for white light emission. *Journal of Display Technology, 12*, 506–512.

48. Hosseini, M. S., & Foroogh, B. (2021). Synthesis and characterization of pure and Dy_2O_3-doped CeO_2 nanoparticles. *The 16th Iranian Chemistry Congress, 7*, 38–42.

49. Dimri, M. C., Khanduri, H., Kooskora, H., Subbi, J., Heinmaa, I., Mere, A., Krustok, J., & Stern, R. (2021). Ferromagnetism in rare earth doped cerium oxide bulk samples. *Physica Status Solidi A, 209*, 353–358.

50. Rui, J., Liu, J., Zhang, T., Peng, Y., et al. (2021). Construction of a ternary Z-scheme In_2S_3@Au@P3HT photocatalyst for the degradation of phenolic pollutants under visible light. *Separation and Purification Technology, 272*, 258–274.

51. Piao, C., Chen, L., Liu, Z., et al. (2021). Construction of solar light-driven dual Z-scheme Bi_2MoO_6/Bi_2WO_6/AgI/Ag photocatalyst for enhanced simultaneous degradation and conversion of nitrogenous organic pollutants. *Separation and Purification Technology, 274*, 119–140.

52. Kamran, M., Yousif, Q. A., Salavati-Niasari, M., et al. (2022). Enhanced photocatalytic degradation of toxic contaminants using Dy_2O_3-SiO_2 ceramic nanostructured materials fabricated by a new, simple and rapid sonochemical approach. *Ultrasonics Sonochemistry, 82*, 105892.

53. Schneider, J., Matsuoka, M., Takeuchi, M., Zhang, J., et al. (2014). Understanding TiO_2 photocatalysis: Mechanisms and materials. *Chemical Reviews, 114*(19), 9919–9986.

54. Sreethawong, T., Chavadej, S., Ngamsinlapasathian, S., & Yoshikawa, S. (2006). A simple route utilizing surfactant-assisted templating sol–gel process for synthesis of mesoporous Dy_2O_3 nanocrystals. *Journal of Colloid and Interface Science, 300*, 219–224.

55. Pan, T.-M., Chang, W.-T., & Chiu, F.-C. (2011). Structural properties and electrical characteristics of high-k Dy_2O_3 gate dielectrics. *Applied Surface Science, 257*, 3964–3968.

56. Chandrasekhar, M., Sunitha, D. V., Dhananjaya, N., Nagabhushana, H., Sharma, S. C., Nagabhushana, B. M., Shivakumara, C., & Chakradhar, R. P. S. (2012). Thermoluminescence response in gamma and UV irradiated Dy_2O_3 nanophosphor. *Journal of Luminescence, 132*, 1798–1806.

57. Chandar, N. K., & Jayavel, R. (2012). Wet chemical synthesis and characterization of pure and cerium doped Dy_2O_3 nanoparticles. *Journal of Physics and Chemistry of Solids, 73*(9), 1164–1169.

58. Kattel, K., Park, J. Y., Xu, W., Kim, H. G., et al. (2012). Paramagnetic dysprosium oxide nanoparticles and dysprosium hydroxide nanorods as T_2 MRI contrast agents. *Biomaterials, 33*(11), 3254–3261.

59. He, B., Zhao, L., Wang, W., Chen, F., & Xia, C. (2011). Electrocatalytic activity of Dy_2O_3 as a solid oxide fuel cell anode material. *Electrochemistry Communications, 13*(2), 194–196.

60. Aung, Y. L., Ikesue, A., Yasuhara, R., & Iwamoto, Y. (2020). Magneto-optical Dy_2O_3 ceramics with optical grade. *Optics Letters, 45*(16), 4615.

61. Strehlow, W. H., & Cook, E. L. (1973). Compilation of energy band gaps in elemental and binary compound semiconductors and insulators. *Journal of Physical and Chemical Reference Data, 2*(1), 163–200.

62. Josephine, G. A. S., & Sivasamy, A. (2014). Nanocrystalline ZnO doped on lanthanide oxide Dy_2O_3: A novel and UV light active photocatalyst for environmental remediation. *Environmental Science & Technology Letters, 1*, 172–178.

63. Hussein, G. A. M., Korban, H., Goda, B., & Miyaji, K. (1997). Physicochemical characterization of the formation course of dysprosium oxide from hydrated dysprosium nitrate; thermoanalytical and microscopic studies. *Colloids and Surfaces A, 125*(1), 63–71.

64. Abkar, E., Hassanpour, M., Amiri, O., Ghanbari, M., & Salavati-Niasari, M. (2021). Photocatalytic and antibacterial activities of Tl–Hg–I nanocomposites: Sonochemical synthesis and characterization. *RSC Advances, 11*, 22238–22249.

65. Salavati-Niasari, M. (2005). Nanoscale microreactor-encapsulation 14-membered nickel (II) hexamethyl tetraaza: Synthesis, characterization and catalytic activity. *Journal of Molecular Catalysis A: Chemical, 229*(1–2), 159–164.

66. Wu, Y., Du, X., Kou, Y., Wang, Y., & Teng, F. (2019). Mesoporous SiO_2 nanostructure: Light-induced adsorption enhancement and its application in photocatalytic degradation of organic dye. *Ceramics International, 45*, 24594–24600.

67. Suwarno, A. C., Yulizar, Y., Apriandanu, D. O. B., & Surya, R. M. (2022). Biosynthesis of Dy_2O_3 nanoparticles using Piper retrofractum Vahl extract: Optical, structural, morphological, and photocatalytic properties. *Journal of Molecular Structure, 1264*, 123–133.

68. Xua, H., Li, H., Sun, G., Xia, J., Wu, C., Ye, Z., & Zhang, Q. (2010). Photocatalytic activity of La_2O_3-modified silver vanadates catalyst for Rhodamine B dye degradation under visible light irradiation. *Chemical Engineering Journal, 160*, 33–41.

69. Xu, A. W., Gao, Y., & Liu, H. Q. (2002). The preparation, characterization, and photocatalytic activities of rare-earth-doped TiO_2 nanoparticles. *Journal of Catalysis, 207*, 151–157.

70. Aponte, A. G., Ramírez, M. A. L., Mora, Y. C., Marín, J. F. S., & Sierra, R. Bu. (2015). Cerium oxide nanoparticles for color removal of indigo carmine and methylene blue solutions. *AIMS Materials Science, 7*(4), 468–485.